RADBOUD UNIVERSITY NIJMEGEN

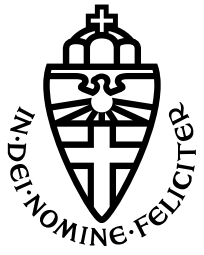

FACULTY OF SCIENCE

A Realistic Look at Secluded Dark Matter

THESIS BSC PHYSICS AND ASTRONOMY

Author:
Simone VAN DER WIJCK

Supervisor:
Dr. Susanne WESTHOFF

Second reader:
Prof. Uli ZEITLER

August 2023

Abstract

In this thesis I have investigated scenarios of a dark matter model where a dark photon is used as a mediator between dark matter and standard model particles, secluded dark matter, in an attempt to find viable dark matter candidates as the fundamental nature of dark matter remains largely unknown. In the secluded dark matter model I researched the two main annihilation channels and focused on dark matter particles with a mass in the GeV scale. I looked at what combinations of values for the variable parameters of these channels could provide realistic dark matter candidates. As the relic density of dark matter has been determined by the Planck Collaboration, this value was compared to the relic density calculated from the proposed dark matter scenarios to check their possibility. From these results I have determined that there are scenarios of the secluded dark matter model that result in the desired relic density, meaning there are realistic candidates of secluded dark matter, and that this can occur through either of the annihilation channels, or a combination of the two.

Contents

1 Introduction

It has been largely accepted that a large percentage of the universe's mass density is contributed by dark matter (DM). However, as one of the defining factors of DM is that it can not easily be detected with telescopes, there are still many questions revolving around the fundamental nature of DM. Answering these questions can lead to a better understanding of the contents and history of the universe.
When investigating DM in the universe, a helpful quantity is the relic abundance, or relic density, of DM. This is the amount of DM remnant from the beginning of the universe and has been determined to a certain precision, with measurements from the Planck Collaboration [1].
This research is interested in using the observed relic abundance to investigate if it is possible to find viable DM candidates belonging to a certain DM model. The DM model is called secluded DM [2]. Specifically, this research focuses on two annihilation channels of the secluded DM particles and their interplay: t-channel annihilation into dark mediators, also referred to as the secluded sector, and s-channel annihilation into Standard Model (SM) particles. By looking at the parameters that influence these interactions and how they lead to the correct relic density, conclusions can be drawn about characteristics of possible DM candidates.
Using the code MicrOMEGAs in combination with parameter scans, possible values and combinations of parameters that characterize the secluded DM model, are investigated [3]. Since it is known what the relic density for DM must be, it can be derived for which ranges of these parameters lead to the best results. These properties can then hopefully be used as a starting point for collider and direct detection searches to further the possible detection of DM.
This thesis will explain the details behind the secluded DM model, as well as clarify how the relic density of DM can be determined in section 2. In section 3, the use of MicrOMEGAs and the method behind the parameter scans will be explained. The results of these parameter scans will be discussed in section 4 and what this could mean for future detection searches is analyzed in section 5.

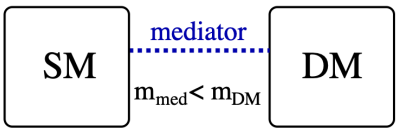

Figure 1: The secluded DM scenario as illustrated in [2].

2 Dark Matter

The existence of DM in the universe has been supported by measurements of the cosmic microwave background (CMB) fluctuations done by WMAP, and later done by Planck, where it has been found that around 85% of the Universe's matter density is contributed by DM [4]. DM implies that there is non-luminous matter in our universe, which can be referred to as either hot, warm or cold. Cold DM (CDM) is non-relativistic and is the type of DM this paper will focus on [5]. How and if DM fits into the SM of particle physics, remains unclear. For this reason, much research is constantly being done in the hopes to gain more insight in the fundamental nature of DM.

2.1 Secluded Dark Matter

Secluded DM is a model in which the DM is decoupled from the SM of particle physics [2]. The secluded DM particles couple to the SM particles through a mediator. This relation is illustrated in Fig. 1.

2.1.1 Annihilation of Secluded Dark Matter

The interactions possible between the DM particles, the mediator and the SM particles can be visualised with the help of Feynman diagrams. From here on out the mediator will be referred to as a dark photon, A'. In Fig. 2 the two fundamental interactions are visualised. In Fig. 2a, two dark matter particles χ interact with the dark photon A', whereas in Fig. 2b two SM particles f interact with the dark photon A'. These interactions come with a specific coupling constant. For the DM interactions with the dark photon, the coupling constant is g_D. For the SM interactions with the dark photon, the coupling constant is ε. From these interactions, two DM annihilation channels can be deduced, as seen in Fig. 3. These annihilation diagrams show two different scenarios. The first, Fig. 3a, can be deduced by taking Fig. 2a twice and classifies DM t-channel annihilation of the secluded sector. Two DM particles annihilate into two dark photons. These dark photons will eventually decay into SM particles. Another possible annihilation can be achieved by combining Fig. 2a and Fig. 2b, resulting in the s-channel annihilation diagram shown in Fig. 3b. In this case, two DM particles annihilate into two SM particles, with the dark photon acting as a 'virtual' particle, meaning the $\chi\chi \rightarrow A'$ interaction cannot be separated from the $A' \rightarrow ff$ interaction. Only if the dark photon is produced as a resonance, do the DM particles annihilate into a dark photon, which

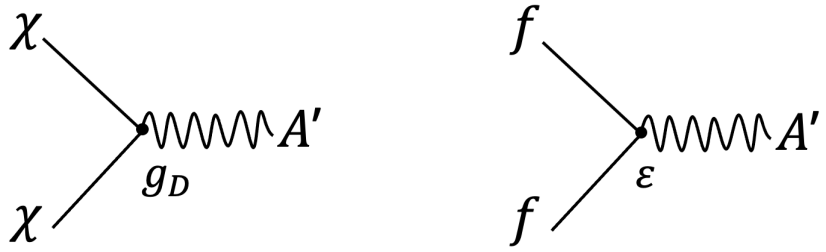

(a) DM interaction. *(b) SM interaction.*

Figure 2: Feynman diagrams of fundamental interactions of DM and SM particles with the dark photon mediator.

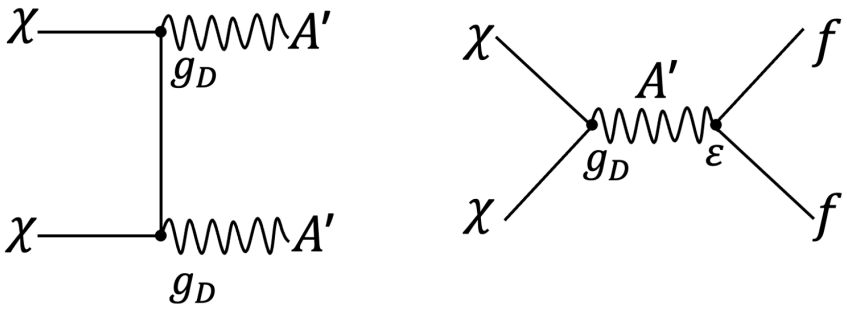

(a) The secluded sector *(b) The s-channel*

Figure 3: Feynman diagrams for secluded DM annihilations.

subsequently decays into two SM particles. The dark photon is a resonance when the mass of the dark photon, $m_{A'}$ is around twice as large as the mass of the DM particle, m_χ.
These DM annihilations influence the amount of DM in the universe, given by the DM number density. The amount of annihilations that occur, along with the time frame during which they occur, alters the evolution of the annihilations and thus the DM number density over time. This determines the amount of DM remaining in the universe today, resulting in the relic density of DM.

2.1.2 Forbidden Dark Matter

Kinematically, the annihilation described in the secluded sector, visualised in Fig. 3a, can only occur when the mass of the DM particle m_χ, is larger than the mass of the dark photon $m_{A'}$. This is noted in Fig. 1 as $m_{med} < m_{DM}$ and is usually a boundary condition for when DM annihilates into the mediator, dark photons. However, there is a scenario in which annihilations can occur when $m_{A'} \gtrsim m_\chi$. Temperature effects of the early universe make it possible that DM particles can annihilate into dark photons with a slightly larger mass. When this is the case, the DM scenario is referred to as forbidden DM.

2.2 Thermal History of Dark Matter

In the early universe SM particles were in thermal equilibrium [6]. This can be reached when the interaction rate of a particle species Γ is much larger than the expansion rate of the universe H, $\Gamma \gg H$, with H also referred to as the Hubble rate. The interaction rate of particles is

$$\Gamma \equiv n\sigma v, \tag{1}$$

where n is the number density, σ is the interaction cross section and v is the average relative velocity of particles. The Hubble rate, or the expansion rate of the universe, is

$$H = \frac{\dot{a}}{a}, \tag{2}$$

with a the scale factor and $\dot{a}$ the time derivative of the scale factor.
If the particle interaction rate is much larger than the Hubble rate, it is implied that for the time scale of particle interactions

$$t_c \equiv \frac{1}{\Gamma} << t_H \equiv \frac{1}{H}, \tag{3}$$

meaning local thermal equilibrium is reached before the effects of the expansion are noticed. However, as the universe expands it also cools. As a result particles interact and annihilate less, decreasing the interaction rate Γ. At a certain point $t_c \sim t_H$ and the particle interaction rate becomes frozen in time as the particles decouple from the thermal bath. This process of particle freeze-out is visualised in Fig. 4. The shape of the graph can be clarified by looking at the distribution function, the number of particles per unit volume in phase space. As particles reach a state of maximum entropy, their phase space distribution is given by

$$f(E) = \frac{1}{e^{-E/T} \pm 1}, \tag{4}$$

with the + sign used for fermions and the − sign for bosons. This distribution becomes exponentially suppressed, $f \to e^{-m/T}$, as the particles with mass m become non-relativistic due to the temperature dropping below the particle mass, $T << m$. If particles kept interacting, they would follow the dotted equilibrium line in Fig. 4. However, due to freeze-out the particle interaction rate becomes constant resulting in the relic density, represented by the solid line in Fig. 4.

2.3 Evolution of Dark Matter Density

2.3.1 Boltzmann Equation

To describe the evolution of the phase-space density of a DM particle in and beyond equilibrium, the Boltzmann equation can be used. The Boltzmann equation says

$$L[f] = C[f], \tag{5}$$

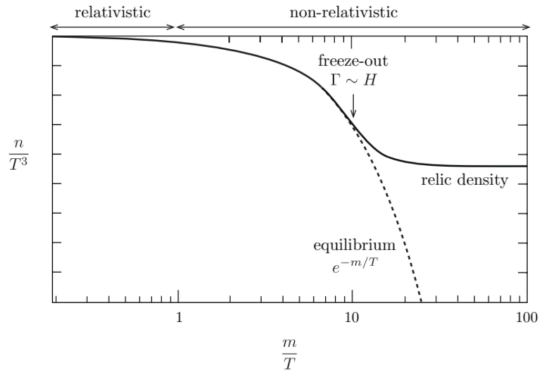

Figure 4: A schematic illustration of particle freeze-out [6].

where $L[f]$ is the Liouville operator and $C[f]$ is the collision operator. The Liouville operator gives the net rate of change in time of the particle phase-space density f, while the collision operator describes the number of particles per phase-space volume that are lost or gained per unit time under collision with other particles [7]. With the use of *Lectures on Dark Matter Physics* by Mariangela Lisanti, an expression for the Boltzmann equation, when applied to DM particles, can be derived [8].
The Liouville operator can be written in terms of the particle energie E, momentum p and time t resulting in

$$L[f] = \frac{\partial f}{\partial t} - H|p^2|\frac{\partial f}{\partial E}, \tag{6}$$

when using the Friedmann-Robertson-Walker cosmological model where the phase-space density is spatially homogeneous and isotropic. The expression of the operator can be rewritten by using the equation for the number density of a given particle species

$$n = \int dn = g\int f(E,t)\,\frac{d^3p}{(2\pi)^3}, \tag{7}$$

where g is the number of degrees of freedom and f is the phase space density of a particle. The Liouville term then becomes

$$g\int L[f]\frac{d^3p}{(2\pi)^3} = \frac{1}{a^3}\frac{d}{dt}\left(na^3\right) = \frac{dn}{dt} + 3Hn, \tag{8}$$

where eq. 2 has been used to relate the scale factor back to the Hubble rate.
To include the collision term, the type of allowed interactions must be clarified. When only considering interactions such as $1+2 \leftrightarrow 3+4$, as interactions between 3 or more particles are highly unlikely [6], the collision term for particle 1 is

$$g_1\int C[f_1]\frac{d^3p_1}{(2\pi)^3} = -\sum_{spins}\int [f_1 f_2\left(1\pm f_3\right)\left(1\pm f_4\right)|\mathscr{M}_{12\to 34}|^2 - f_3 f_4\left(1\pm f_1\right)\left(1\pm f_2\right)|\mathscr{M}_{34\to 12}|^2]$$

$$\times (2\pi)^4 \delta^4\left(p_1 + p_2 - p_3 - p_4\right) d\prod_1 d\prod_2 d\prod_3 d\prod_4, \tag{9}$$

where the sum is over initial and final spins [7], the + and − signs in $1 \pm f_i$ represent bosons or fermions respectively, $\mathscr{M}$ are the invariant polarized amplitudes obtained with the Feynman rules, the delta function enforces energy and momentum conservation and

$$d\prod_i = \frac{d^3 p_i}{(2\pi)^3 2E_i} \tag{10}$$

are the phase-space integration factors.
With assumptions, eq. (9) can be reduced to a more manageable expression. Firstly, from Fig. 3 it can be concluded that particles 1 and 2 in eq. (9) are identical DM particles. Furthermore, it must be assumed that particles 3 and 4 are in equilibrium with the thermal background quickly after the interaction. Besides that, the phase-space distribution can take on the Fermi-Dirac or Bose-Einstein expressions if the particles remain in kinetic equilibrium. Lastly, the temperature must satisfy $T_i << E_i - \mu_i$, with μ_i the chemical potential, so that $\left(1 \pm f\right) \sim 1$. This is the case as the temperature dependence follows the Maxwell-Boltzmann distribution.
This results in

$$\sum_{spins} \int |\mathscr{M}_{ij\to kl}|^2 \times (2\pi)^4 \delta^4\left(p_i + p_j - p_k - p_l\right) d\prod_k d\prod_l = 4 g_i g_j \sigma_{ij} \sqrt{\left(p_i \cdot p_j\right)^2 - \left(m_i m_j\right)^2}, \tag{11}$$

where the following definition is used to relate the cross section for the scattering process σ_{ij} to the matrix element $\mathscr{M}$ [9],

$$d\sigma_{ij} = \frac{|\mathscr{M}_{ij\to kl}|^2}{4 g_i g_j \sqrt{\left(p_i \cdot p_j\right)^2 - \left(m_i m_j\right)^2}} (2\pi)^4 \delta^4\left(p_i + p_j - p_k - p_l\right) d\prod_k d\prod_l. \tag{12}$$

The collision term then becomes

$$g_1 \int C[f_1] \frac{d^3 p_1}{(2\pi)^3} = -\int \left(\sigma v_{m\phi l}\right)_{12} dn_1 dn_2 - \left(\sigma v_{m\phi l}\right)_{34} dn_3 dn_4, \tag{13}$$

where dn is defined in eq. 7 and $v_{m\phi l}$ is the Møller velocity for an $ij \to kl$ process given by

$$\left(v_{m\phi l}\right)_{ij} = \frac{\sqrt{\left(p_i \cdot p_j\right)^2 - \left(m_i m_j\right)^2}}{E_i E_j}. \tag{14}$$

The Møller velocity is defined in such a way that $\left(v_{m\phi l}\right)_{ij} n_i n_j$ is invariant under Lorentz transformations. As $\sigma v_{m\phi l}$ varies slowly when the number density of the initial and final-state particles change, it can be taken out of the integral.
When setting the Liouville operator of eq. 8 equal to the collision operator of eq. 13, all that is left is

$$\dot{n}_1 + 3Hn_1 = -\langle \sigma v_{m\phi l} \rangle_{12} n_1 n_2 + \langle \sigma v_{m\phi l} \rangle_{34} n_3 n_4, \tag{15}$$

where $\dot{n}$ is the time derivative of the particle number density and $\langle \sigma v_{m\phi l} \rangle$ is the thermally averaged total annihilation cross section times the Møller velocity. It can also be defined as

$$\langle \sigma v_{m\phi l} \rangle_{ij} = \frac{\int \sigma v_{m\phi l} dn_i^{eq} dn_j^{eq}}{\int dn_i^{eq} dn_j^{eq}}, \tag{16}$$

with n^{eq} the equilibrium values of the particle number densities [7]. To simplify notation $v_{m\phi l}$ will be written as v from here on out.
As particles 3 and 4 are assumed to be in thermal equilibrium with the thermal bath, if the identical DM particles 1 and 2 are assumed to be in equilibrium with particles 3 and 4, detailed balance states

$$\langle \sigma v \rangle_{12} n_{eq}^2 = \langle \sigma v \rangle_{34} n_3^{eq} n_4^{eq}, \tag{17}$$

so that the Boltzmann equation becomes

$$\dot{n} + 3Hn = \langle \sigma v \rangle \left(n_{eq}^2 - n^2 \right) \tag{18}$$

where $\langle \sigma v \rangle = \langle \sigma v \rangle_{12}$. Therefore, the Boltzmann equation is defined by the DM number density n, the DM number density in equilibrium n_{eq}, the Hubble rate H and the thermally averaged total annihilation cross section times the Møller velocity $\langle \sigma v \rangle$.

2.3.2 Boltzmann Equation for Forbidden Dark Matter

This Boltzmann equation, eq. 18, has been set up with the assumption that the DM particles annihilate into two lighter particles. When looking at forbidden DM, where the two annihilation products have a larger mass $m_{A'} > m_\chi$, the equation changes slightly to

$$\dot{n}_\chi + 3Hn_\chi = -\left(\langle \sigma v \rangle\right)_{\chi\chi} n_\chi^2 + \left(\langle \sigma v \rangle\right)_{A'A'} \left(n_{A'}^{eq} \right)^2, \tag{19}$$

with n_χ the DM number density and $n_{A'}$ the dark photon number density in equilibrium.

2.3.3 Rescaled Boltzmann Equation

The universe expands, decreasing the DM number density n. This effect can be scaled out by introducing $Y = n/s$, with s the total entropy density of the universe. Using $sa^3 = constant$ so that $\dot{s} = -3sH$, the Boltzmann equation (eq. 18) rescaled is

$$\frac{dY}{dt} = \langle \sigma v \rangle s \left(Y_{eq}^2 - Y^2 \right). \tag{20}$$

A rescaled time variable can be introduced as well, $x = m_\chi / T$ with m_χ the DM particle mass, as the more interesting dynamics occur when $T \sim m_\chi$. In this case we need

$$\frac{dx}{dt} = \frac{d}{dt}\left(\frac{m_\chi}{T} \right) = -\frac{1}{T}\frac{dT}{dt} x \simeq Hx. \tag{21}$$

Assuming $T \propto a^{-1}$ for times relevant to freeze-out [6] results in

$$\frac{dY}{dt} = -\frac{xs\langle\sigma v\rangle}{H(m)}\left(Y_{eq}^2 - Y^2\right). \tag{22}$$

The expression that remains describes the evolution of the DM density, rescaled to remove the effects of the expanding universe and depends strongly on the velocity-averaged cross section $\langle\sigma v\rangle$. Unfortunately there are no analytical solutions for eq. 22, so numerical solutions must be found to get exact results. Intuitively, the evolution of the DM number density Y over time can be investigated. If x_f is the freeze-out time, then $Y\left(x \lesssim x_f\right) \simeq Y_{eq}(x)$ and $Y\left(x \gtrsim x_f\right) \simeq Y_{eq}\left(x_f\right)$. This means that before the time of freeze-out $Y(x)$ decreases exponentially and after freeze-out it remains constant at a larger value than if freeze-out had not occurred.

2.4 Relic Density

With the DM abundance today Y_{today}, an expression for the fraction of the critical density $\rho_{critical}$ contributed by the DM today can be made. This is known as the relic density or relic abundance and is given by

$$\Omega_\chi = \frac{ms_{today}Y_{today}}{\rho_{critical}}, \tag{23}$$

often denoted as $\Omega_\chi h^2$

$$\Omega_\chi h^2 \sim \frac{10^{-26} cm^{-3}/s}{\langle\sigma v\rangle}. \tag{24}$$

A value for $\Omega_\chi h^2$ has been determined as

$$\Omega_\chi h^2 = 0.120 \pm 0.001, \tag{25}$$

from the final full-mission Planck measurements of the CMB anisotropies [1].

2.4.1 Variables for determining the Relic Density

To see if the secluded DM model could result in possible DM candidates, the model needs to deliver a relic density that matches the value determined by Planck. To determine this, a closer look is needed at the variables in the secluded DM model that influence the relic density. Eq. 24 shows that the relic density is inversely proportional to the velocity-averaged cross section $\langle\sigma v\rangle$. The cross section in turn, is dependent on the type of annihilation that takes place. For the secluded sector (Fig. 3a), the cross section has the dependence

$$\sigma \sim \alpha_D^2 \sqrt{1 - \frac{m_{A'}^2}{m_\chi^2}} \cdot \frac{1}{m_\chi^2}, \tag{26}$$

where m_χ is the DM particle mass, $m_{A'}$ is the dark photon mass and $\alpha_D = g_D^2/(4\pi)$ is a rescaled expression of the coupling constant for DM interactions with dark photons [2]. For the s-channel annihilation (Fig. 3b) the relation is a little different with

$$\sigma \sim \alpha_D \varepsilon^2. \tag{27}$$

When looking at the dependence on the DM particle and dark photon masses for the s-channel annihilation, σ scales with

$$\sigma \sim \frac{1}{m_\chi^2} \text{ when } m_\chi \gg m_{A'} \tag{28}$$

and

$$\sigma \sim \frac{m_\chi^2}{m_{A'}^4} \text{ when } m_{A'} \gg m_\chi. \tag{29}$$

This means that the variables that define the relic density based off of these two DM annihilation channels are m_χ, $m_{A'}$, α_D and ε. The cross section σ is also a way to determine the probability that a specific annihilation channel will determine the relic abundance.

```
==== Calculation of relic density =====
Xf=2.22e+01 Omega=1.20e-01
# Channels which contribute to 1/(omega) more than 1%.
# Relative contributions in % are displayed
  100% ~Chi2 ~Chi2~ ->Ap Ap
```

Figure 5: MicrOMEGAS output for the relic density (Omega = Ωh^2) with input values $m_\chi = 2.01GeV$, $m_{A'} = 0.55GeV$, $\alpha_D = 10^{-4}$ and $\varepsilon = 10^{-5}$.

3 Calculating the Relic Density with MicrOMEGAs

To calculate the relic density of a DM model, MicrOMEGAs_5.3.4.1 can be used in combination with a Feynrules model for inelastic Dirac DM [10]. MicrOMEGAs includes all channels of annihilation and coannihilation of stable, massive particles in its calculations [11]. The Feynrules model contains information describing the particles, their interactions and the parameter values. Based on the parameter input values, MicrOMEGAs will calculate a relic density output which can then be compared to the value determined by Planck and WMAP. If the values match, the parameters could correspond to a possible DM candidate. MicrOMEGAs will also note the percentage of the relic denity contributed by a certain type of annihilation channel. A possible output of micrOMEGAs can be seen in Fig. 5. There, it can be seen that the input values result in a value for the relic density of $\Omega h^2 = 0.120$ and that 100% of the interactions that took place were secluded sector annihilations of $\chi\chi \rightarrow A'A'$, where in MicrOMEGAs χ is denoted with $Chi2$ and A' is given with Ap.
With different combinations of values for the parameters, different relic density outputs can be found. However, an array of combinations for the parameters could also lead to the same, correct, relic density value. The goal is to find these combinations of parameter values that correspond to a correct relic density output. To do this, certain boundary conditions of parameter values must be kept in mind. Firstly, this research is interested in the GeV scale of the DM particle mass so that the resulting dark photons are potentially long-lived particles with interesting chances for detection. To ensure the particles remain non-relativistic and in line with prior discoveries the limit is set $10MeV \leq m_\chi \leq 2GeV$. The minimum value comes from strong bounds from astrophysics. The maximum value is because when DM has a larger mass, it will freeze out during the QCD phase transition which is difficult to predict. Setting an allowed range for the DM mass, influences the dark photon mass. For secluded sector annihilations, the dark photon mass can not be much larger than the DM mass, as that results in forbidden DM. Moreover, from the BaBar experiment it has been found that $\varepsilon \lesssim 10^{-3}$ [12]. Finally, to ensure the particles remain in thermal equilibrium $g_D\varepsilon \geq 10^{-7}$ meaning $\alpha_D \geq 10^{-8}$.

3.1 Parameter Scans with ABC Code

To find the arrays of different parameter value combinations, parameter scans can be performed. This has been done using an Artificial Bee Colony (ABC) code. The ABC code scans over an inputted range of values for parameters and finds the combinations of those parameters that result in the desired output value. For the case of secluded DM, a relic density output value of $\Omega h^2 = 0.120 \pm 0.001$ is wanted. However, for this research the allowed range has been extended to $\Omega h^2 = 0.120 \pm 0.003$ to leave some room for error.
The ABC code functions by setting the amount of 'bees' and 'tries', as well as deciding the parameter ranges. When running the code, the 'bees' become randomized data points within the chosen ranges. The code then chooses another random data point that lies between two different bees. If the data point has a result closer to the desired relic density, one of the bees will change its values to that of the new data point. If the result is not better, the bee does not change. In this manner, the code will run through all the bees. The amount of tries determines how often a bee can not change due to the result not being better, before the bee is 'reset' and gets a new set of values.
To be able to present the gathered data in plots, the code is limited to scanning over two variable parameters at the same time. As there are four variables in the secluded DM model, two of the four will always have to be kept constant. This means that there are multiple combinations of variable parameters possible, each bringing new insight in the possibilities for secluded DM.

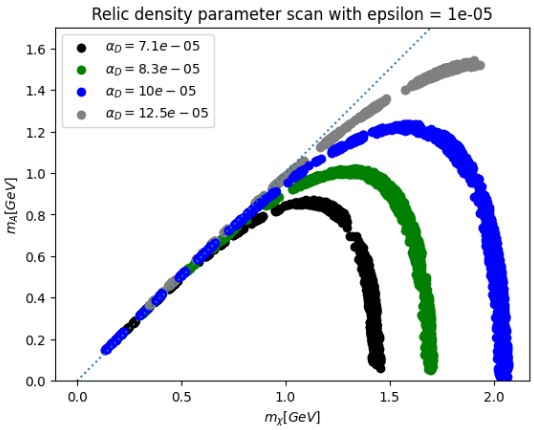

(a) DM mass plotted against the dark photon mass.

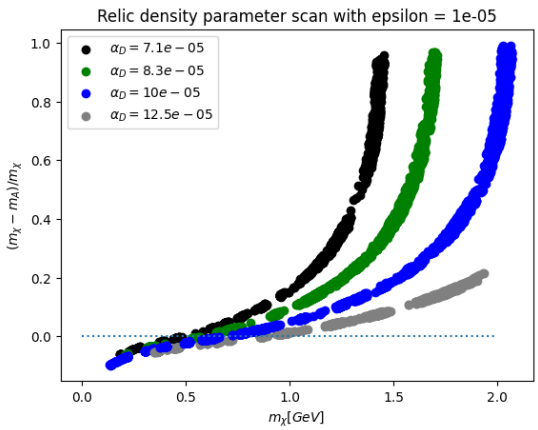

(b) DM mass against relative mass difference.

Figure 6: The relation between the dark matter particle mass m_χ and the dark photon mass $m_{A'}$ for a fixed ε and various fixed α_D values.

4 Results of the Parameter Scans

4.1 Mass versus α_D in the Secluded Sector

To look at the relation between parameters of DM annihilations that take place purely in the secluded sector, meaning interactions of 100%$\chi\chi \to A'A'$, the coupling constant ε has to be to set to a small value. This ensures that the s-channel interaction is switched off as α_D has stronger coupling than ε in the annihilations. The relations laid out in eq. 26 and 27 show how the size of ε can have an effect on the cross section. If ε is around the same order of magnitude of α_D, the cross section for the s-channel annihilation will be much smaller meaning it is more probable that secluded sector annihilations will take place.
Through initial scans it was determined that to get the correct results for the relic density exclusively from secluded DM, for the chosen DM particle mass range, α_D has to be of the order of magnitude of 10^{-5}. For this reason, ε was set to $\varepsilon = 10^{-5}$, ensuring all annihilations take place through secluded sector interactions. Parameter scans were then completed to find the allowed combinations of m_χ and $m_{A'}$ for different set values of α_D. Four α_D values were chosen to show how the mass pairings evolve as α_D increases.
In Fig. 6 two plots are shown, where the DM particle mass is plotted against the dark photon mass (Fig. 6a) and the relative mass difference (Fig. 6b). The graphs (and all graphs that follow) can be seen as continuous, as the small gaps are a consequence of how the parameter scans were performed. For smaller DM particle masses, at these α_D values, it is clear that the annihilations are of forbidden dark matter as the relative mass difference is negative, visible in Fig. 6b. As the DM mass increases, the correlating dark photon mass increases, until a certain maximum. After that point the dark photon mass starts to decrease quickly. The cause of this turnover can be related back to number density. As the DM particle mass increases, freeze-out will happen later due to the exponential suppression of the number

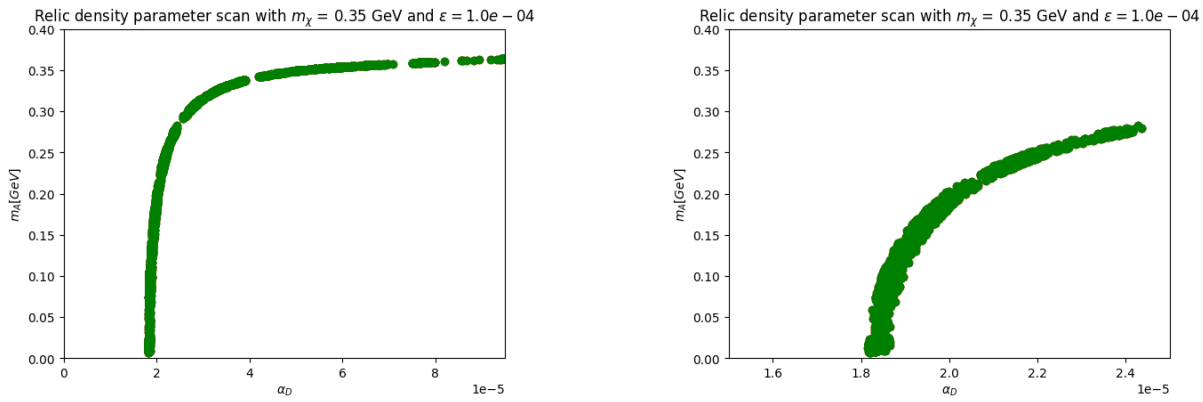

Figure 7: The dependence on α_D for a fixed ε and fixed dark matter particle mass m_χ as the dark photon mass m_A varies, with the right plot giving a closer look at the α_D dependence for $m_A < 0.3GeV$.

density. To compensate this suppression so that the correct relic density is still found, the cross section must be made more efficient by lowering the dark photon mass through eq. 26. When it comes to the changes in α_D, as α_D increases, the maximum DM mass and dark photon mass allowed increases as well. This again reverts back to the relation in eq. 26. As the $m_{A'}$ or m_χ increases, the cross section will decrease. To compensate this change so that the correct relic density value is still achieved, α_D needs to increase.
It is also worth noting that it appears the relic density is very sensitive to changes in α_D, as a change in α_D of $3 \cdot 10^{-5}$ already causes the maximum DM particle mass to shift by $0.5GeV$. This again is related back to 26, as $\sigma \sim \alpha_D^2$ shows that a small change in α_D will impact the cross section and therefore the relic density, resulting in a shift of either the dark matter or the dark photon mass to counterbalance the change.

4.2 Dark Photon Mass versus α_D

When looking to see when the s-channel interactions will take place along with the secluded sector annihilations, α_D as well as ε need to be altered. That is why parameter scans were performed to investigate the influence of ε and α_D on the annihilations, and thus the relic density, for a fixed DM particle mass m_χ while varying the dark photon mass $m_{A'}$. It was found that at least for $\varepsilon \leq 10^{-4}$, the annihilations were described as $100\%\chi\chi \rightarrow A'A'$ annihilations, meaning the interactions are all in the secluded regime.
The results of the scans with $\varepsilon = 10^{-4}$ and $m_\chi = 0.35GeV$ can be seen in Fig. 7. A value of $m_\chi = 0.35GeV$ was chosen as there should then be multiple α_D and $m_{A'}$ combinations that would lead to the correct relic density. This can partially be determined from Fig. 6, as it shows that there are relic density results for forbidden DM at the chosen DM mass value with the set α_D values. From Fig. 6 it can also be predicted that there should be DM interactions that lead to the correct relic density for smaller α_D values than those shown in the figure.
When looking at the results of Fig. 6 and 7, some conclusions can be drawn for the secluded

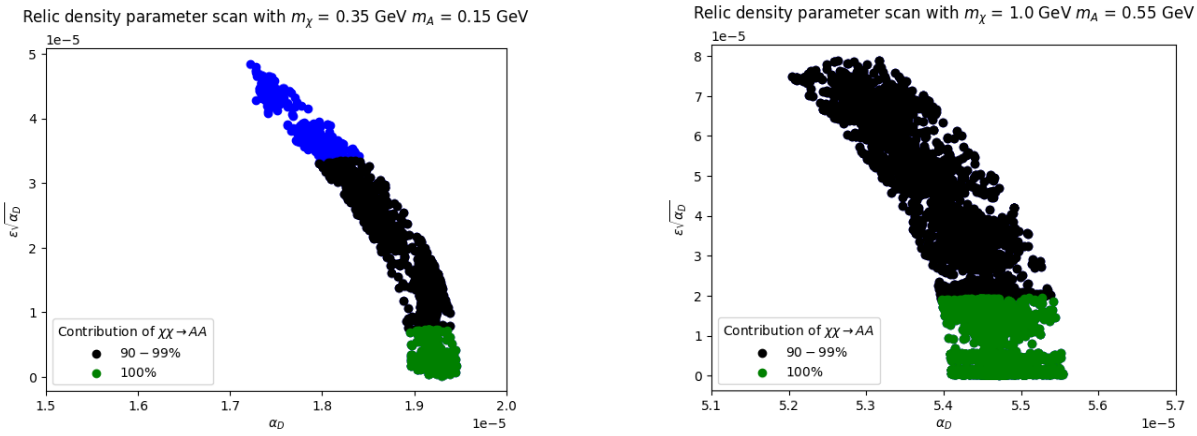

(a) *(b)*

Figure 8: A look at how the interactions change as α_D and ε are varied, for a fixed dark matter particle-dark photon pairing.

regime annihilations. Firstly, for the interactions where $m_\chi \gtrsim m_{A'}$, there is a very small range for α_D values that results in the correct relic density when m_χ and ε is fixed. This is clearly visualised in Fig. 7 where α_D remains just under $2e-05$ while $m_{A'} \lesssim 0.30GeV$. There are some minor shifts in α_D that arise due to changes in $m_{A'}$, which can be seen in the right plot of Fig. 7. This sensitivity to α_D in the secluded sector when m_χ and ε are fixed, is in line with the discussion of Fig. 6 in section 4.1. As the secluded sector cross section has a stronger dependence on α_D than it does on $m_{A'}$, a more noticeable increase in the dark photon mass can be seen while α_D has a relatively small increase.
Once $m_\chi \lesssim m_{A'}$, the annihilations start including forbidden DM and the dependency on α_D changes. In Fig. 6 this is visualised by the graphs with different α_D values overlapping when the DM mass is similar or slightly smaller than the dark photon mass. This means that there are many possible α_D values for the forbidden DM mass combinations. This is further confirmed in Fig. 7, where the graph converges as $m_{A'}$ surpasses the set value of $m_\chi = 0.35GeV$. Therefore a much larger α_D range results in the correct relic density for forbidden DM, compared to when $m_\chi \gtrsim m_{A'}$.

4.3 α_D versus ε for Different Fixed Mass Pairings

Another way to investigate the interplay between the secluded sector and the s-channel annihilations, is to vary ε along with α_D for fixed mass pairings, meaning $m_{A'}$ is kept constant together with m_χ, in such a way that the effects of the coupling constants can be evaluated. For this reason, the results of these parameter scans are visualised in plots with the secluded sector and s-channel couplings defining the axis. While the secluded sector only depends on the coupling α_D as defined in eq. 26, the cross section of the s-channel annihilations, eq. 27, depend on both α_D and ε. To plot the found pairings of α_D and ε that give the correct relic density in such a way that the results correspond to the respective annihilation couplings,

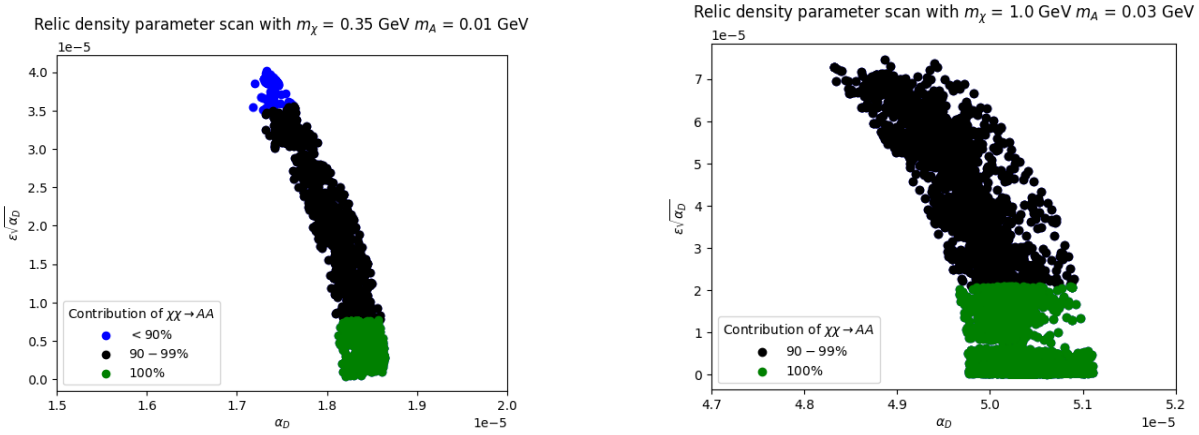

(a) *(b)*

Figure 9: A look at how the interactions change as α_D and ε are varied, for a fixed dark matter particle-dark photon pairing, with a relatively small dark photon mass to remove phase-space suppression.

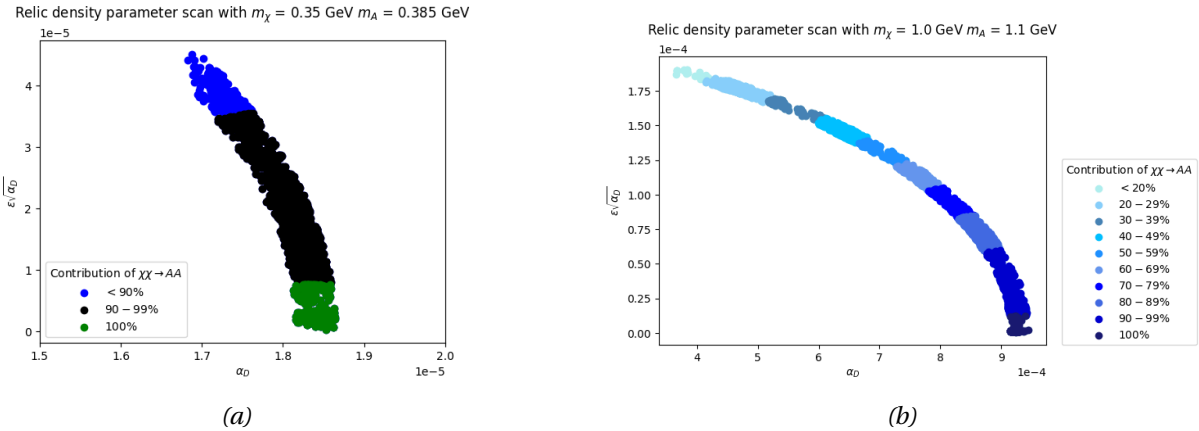

(a) *(b)*

Figure 10: A look at how the interactions change as α_D and ε are varied, for a fixed dark matter particle-dark photon pairing in the forbidden region.

the data has been plotted in graphs with α_D on the x-axis and $\varepsilon\sqrt{\alpha_D}$ on the y-axis. These results are shown in Fig. 8, Fig. 9 and Fig. 10.
The dark matter mass m_χ was kept constant at $0.35GeV$ as well as $1GeV$. The first DM particle mass was chosen so that the results of section 4.2 could be used as a starting point for a value of α_D in the paramter scans. The second DM mass value of $1GeV$ was chosen to see how the interactions and dependencies on α_D and ε wound change for a larger DM mass that still falls within the set DM particle mass bounds. For each DM mass, three different relative dark photon mass scenarios were chosen: one where the the relative mass difference is around half, one where the dark photon mass is much smaller than the DM mass, and one where the dark photon mass is slightly larger than the DM mass resulting in forbidden DM. In the first scenario, Fig. 8, the dark photon masses are set at $m_{A'} = 0.15GeV$ for $m_\chi = 0.35GeV$ and $m_{A'} = 0.55GeV$ for $m_\chi = 1.0GeV$. In the second, Fig. 9, the dark photon masses are much smaller than the DM masses, with $m_{A'} = 0.01GeV$ for $m_\chi = 0.35GeV$ and $m_{A'} = 0.03GeV$ for $m_\chi = 1.0GeV$. Lastly, in Fig. 10, $m_{A'} = 0.385GeV$ is chosen for $m_\chi = 0.35GeV$ and $m_{A'} = 1.1GeV$ for $m_\chi = 1.0GeV$ to include a scenario that deals with forbidden DM.
Previously, a boundary of $\varepsilon < 10^{-3}$ was set due to observations. From the initial parameter scans it became clear that the annihilations remained fairly similar below that boundary. To see if theoretically this would change if ε increased, the boundary was extended to 10^{-2}. This boundary set on the allowed values for ε means that there is a boundary on the obtained values of $\varepsilon\sqrt{\alpha_D}$ as well. For the figures 8, Fig. 9 and Fig. 10, it seems as though there should be more results for the top left of the plots, however the graphs are cut of due to the set boundary condition on ε.
When looking at the results with $m_\chi = 0.35GeV$, from Fig. 8a, 9a and 10a it is evident that α_D only becomes more restricted as a fixed mass pairing is set. In all the scenarios the α_D values seem to be fairly similar, around 1.9e-05, regardless of the dark photon mass. However, a slight decrease in α_D is seen as $\varepsilon\sqrt{\alpha_D}$ increases in each of the respective figures. The severity of this decrease varies slightly for each of the dark photon mass values. The value of α_D shifts a little as well, when looking at the same $\varepsilon\sqrt{\alpha_D}$ values for the different mass pairings. Nevertheless, these variations of α_D are still of the order 10^{-6}. These slight changes in α_D and $\varepsilon\sqrt{\alpha_D}$ can be seen as a shift in the efficiency of the annihilations from the secluded sector to the s-channel as the s-channel annihilations start contributing more to the relic abundance. These three figures show that for $\varepsilon < 10^{-3}$ the allowed annihilations are dominated by the secluded sector annihilations. Only after around $\varepsilon = 2 \cdot 10^{-3}$ are the interactions no longer $100\%\chi\chi \to A'A'$, and after $\varepsilon = 8 \cdot 10^{-3}$ does this decreases further to below $90\%\chi\chi \to A'A'$. In section 4.1 it was already determined by looking at equations 26 and 27 that ε must be larger than α_D for the s-channel interactions to dominate with these specific relative mass pairings. However, through 8a, Fig. 9a and Fig. 10a it is clear how much larger ε must be compared to α_D for the s-channel interactions to start contributing to the relic density, in regards to these specific mass values.
The same can be said when looking at the results gathered with $m_\chi = 1.0GeV$ paired with $m_{A'} = 0.55GeV$ and $m_{A'} = 0.03GeV$. Only in the scenario of forbidden DM with $m_\chi = 1.1GeV$

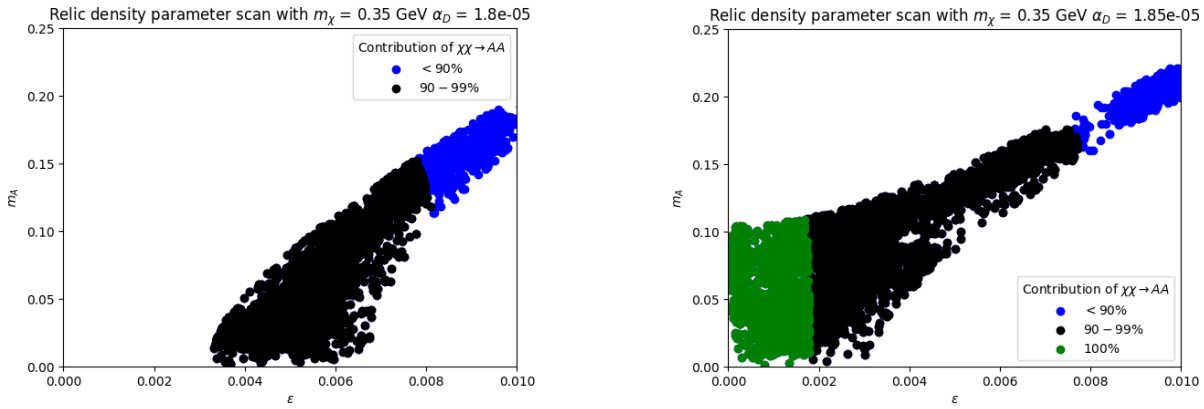

(a) *(b)*

Figure 11: A look at how the interactions change as ε and $m_{A'}$ are varied, for a fixed dark matter particle mass and α_D.

do the results look significantly different.
In figures 8b and 9b, the results are similar to those in 8a and 9a. There is only a slight variation in the α_D values for the different $m_{A'}$ values, albeit a slightly larger difference compared to the results for when $m_\chi = 0.35GeV$. Moreover, as $\varepsilon\sqrt{\alpha_D}$ increases until the set boundary of $\varepsilon = 10^{-2}$ is reached, the interaction contribution of $\chi\chi \to A'A'$ does not decrease to below 90% as it does for when $m_\chi = 0.35GeV$. This would mean that for these mass pairings, the secluded sector annihilations are much more dominant when it comes to contributing to the correct relic density, compared to the s-channel annihilations.
Fig. 10b is the only figure that deviates from the $m_\chi = 0.35GeV$ equivalent. The results even deviate strongly from the other $m_\chi = 1.0GeV$ results, whereas for $m_\chi = 0.35GeV$ all the graphs remain relatively similar. The forbidden DM mass pairing of Fig. 10b results in α_D values of the order of magnitude 10^{-4} instead of 10^{-5}. Another noticeable difference is that now the interaction contributions do start to change drastically as $\varepsilon\sqrt{\alpha_D}$ increases, going all the way to $< 20\%\chi\chi \to A'A'$ as $\varepsilon = 10^{-2}$. Along with the larger changes in interaction contributions, the results cover a wider range of α_D with the value decreasing as ε increases. To have a better understanding as to why figures 10a and 10b are so different, more parameter scans would have to be performed for forbidden DM in the set DM mass range. However, it could be that as the DM mass, and therefore the dark photon mass, increases, the cross section of the s-channel interaction becomes much more efficient for this mass pairing, resulting in more contributions from s-channel annihilations to the correct relic density.

4.4 ε versus Dark Photon Mass

The annihilations that result in the correct relic density are sensitive to changes in α_D, as is defined in eq. 26 and made visible with the results in sections 4.2 and 4.3. The α_D^2 dependence of the secluded sector cross section results in a strong dependence on this coupling

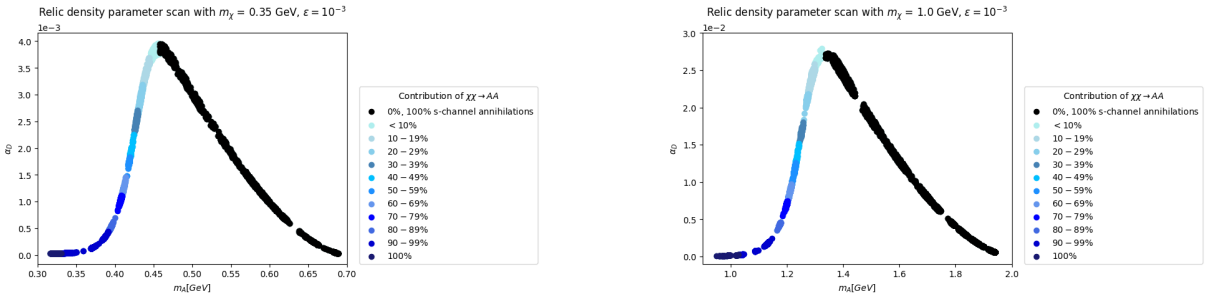

(a) *(b)*

Figure 12: The relation between $m_{A'}$ and α_D for a fixed dark matter particle mass and ε value to see the changeover to fully s-channel annihilations.

when calculating the relic density, especially when the secluded sector annihilations provide the most contributions to the relic density. For this reason, another parameter scan worth investigating is one done with α_D and m_χ fixed while ε and $m_{A'}$ vary, to see how sensitive the relic density is to changes in these variable without the dependence on α_D influencing the results.

Once again, m_χ was kept at $0.35GeV$. The results from these parameter scans can be seen in Fig. 11 where the two values chosen for α_D are $\alpha_D = 1.80 \cdot 10^{-5}$ and $\alpha_D = 1.85 \cdot 10^{-5}$. These values were chosen based off of the results in Fig. 8a, 9a and 10a.

As in section 4.3, the sensitivity to changes in α_D, when the DM mass is fixed, becomes clear. In Fig. 11b, α_D is $5 \cdot 10^{-7}$ larger than the α_D in Fig. 11a, and still there is a larger difference in the values for ε that result in the correct relic density. Moreover, Fig. 11b includes a whole area of 100%$\chi\chi \to A'A'$ interactions, which is missing in Fig. 11a. Interestingly, as ε increases, the allowed dark photon mass increases as well, whereas the range in allowed dark photon masses decreases. This is especially noticeable in Fig. 11b and can be a result of the increase in contributions of s-channel annihilations, as ε increases. As ε increases, the efficiency of the s-channel interactions increases through eq. 27. As the s-channel interactions start contributing more to the relic density, the secluded sector annihilations need to contribute less, to keep the relic density value stable. The increase in the dark photon mass results in a decrease in the secluded sector cross section as per eq. 26, lowering the efficiency of the secluded sector.

4.5 α_D versus Dark Photon Mass to Investigate the S-Channel

A way to investigate when the s-channel interactions will influence the relic density more than the secluded sector annihilations, is by forcing the s-channel to be the more dominant annihilation channel. This can be done by looking at the cases where the dark photon mass is larger than the DM particle mass. As discussed in section 2.1.2, when the dark photon mass is only slightly larger than the DM mass, secluded sector annihilations can still occur through forbidden annihilations. Once the dark photon mass becomes even larger, the interactions

have to occur through the s-channel annihilations.
The s-channel interactions have to dominate at a certain mass difference $m_{A'} - m_\chi$, from a mass pairing perspective. Therefore, it is interesting to investigate what this would mean for the coupling values, especially during the shift from mainly secluded sector annihilations to only s-channel annihilations that influence the relic abundance as the dark photon mass increases.
For this reason, parameter scans were done with α_D and the dark photon mass $m_{A'}$ as variables, while the DM particle mass m_χ and ε were set as constants. For the DM mass the two values $m_\chi = 0.35GeV$ and $m_\chi = 1.0GeV$ were chosen, to be able to compare the results to those from the previous sections. For ε the value $\varepsilon = 10^{-3}$ was set, as this is the maximal value for this coupling acoording to the bounds set by the BaBar experiment and the s-channel interactions are more efficient when ε is larger.
The dark photon mass ranged from just under m_χ to near $2m_\chi$ for each DM mass value. The minimal value ensures that the interaction types range from $100\%\chi\chi \rightarrow A'A'$, all the way to exclusively s-channel interactions meaning the transitions of interaction types can be visualised. For $m_\chi = 0.35GeV$, the purely secluded sector results were visualised in Fig. 7. The maximal dark photon mass value was determined as near the range of $2m_\chi$, the α_D values become so small that the fluctuations will not be seen anymore when using the scale necessary to investigate the transitions in the annihilation type.
The results of these parameter scans can be seen in Fig. 12. In both plots a clear transition can be seen from fully secluded sector annihilations to fully s-channel annihilations, with a continuous decrease of the contribution from secluded sector annihilations to the relic density connecting the two.
Both plots in Fig. 12 are very similar in shape, regardless of there DM particle mass. They both start with relatively small α_D values, as the annihilations taking place consist of $100\%\chi\chi \rightarrow A'A'$ interactions. Whats follows is a strong increase in α_D as $m_{A'}$ increases, until it reaches a maximum. During the mass increase, the total contribution to the relic density by the secluded sector interactions steadily decreases until those types of annihilations no longer take place. For both DM masses, the maximum occurs when the relative mass difference is around 0.31. At the maximum, there is a change in transition types, where there are no longer any contributions by secluded sector annihilations. After the maximum, α_D decreases again as the dark photon mass increases, and all the interactions occur through the s-channel.
The initial increase in α_D can be attributed to the fact that the secluded sector annihilations still plays a part. It seems that as the efficiency of the secluded sector annihilations decrease as they go further into the forbidden regime, α_D increases to compensate this loss. An increase in α_D results in an increase in the cross section, as per eq. 26, meaning the interactions are more likely to occur through that channel, However, at the same time the s-channel interaciton cross section is increasing, as per eq. 27, as the s-channel interactions are becoming more and more dominant. Moreover, even though the secluded sector cross section is increasing, $m_{A'}$ is increasing as well and at a certain point the dark photon mass is too large compared to the DM particle mass. Even with the temperature effects of the early universe, the interactions can no longer happen as forbidden DM through the secluded sec-

```
==== Calculation of relic density =====
Xf=2.00e+01 Omega=1.20e-01
# Channels which contribute to 1/(omega) more than 1%.
# Relative contributions in % are displayed
   33% ~Chi2 ~Chi2~ ->u u~
   25% ~Chi2 ~Chi2~ ->e- e+
   25% ~Chi2 ~Chi2~ ->m- m+
    8% ~Chi2 ~Chi2~ ->d d~
    8% ~Chi2 ~Chi2~ ->s s~
```

Figure 13: MicrOMEGAs output for the relic density from s-channel annihilations exclusively, and a list of the interactions that contributed.

tor. The s-channel interactions will take over completely and be the only kind of annihilation contributing to the calculations of the relic density. Once this change takes place, α_D starts to decrease again as the dark photon mass increases. The reasoning for this change could have to do with the fact that as $m_{A'}$ increases, it starts to come closer to $2m_\chi$ and therefore the resonance regime. As a result, the efficiency of the s-channel annihilations increases and the value of α_D can decrease.
Another important detail is that for the two different DM particle masses, the order of magnitude of α_D changes. The values of α_D are larger when the DM particle mass is larger as well. For the secluded sector interactions this relates back to eq. 27, and is in line with the discussion in section 4.1.
Lastly, when looking at the type of interactions that contribute to the relic density through s-channel interactions, for both m_χ values the distribution is that listed in Fig. 13. Noticeably, the contributions of $\chi\chi \to uu$ are four times larger than those of $\chi\chi \to dd$ and $\chi\chi \to ss$ as the dark photon couples to the electric charge Q. This observation can be related back to the fact that the cross section scales as

$$\sigma \sim \frac{Q_u^2}{Q_d^2} = \frac{(2/3)^2}{(1/3)^2} = 4. \tag{30}$$

4.5.1 Resonance Regime

When investigating the possible parameter values for α_D and $m_{A'}$ for a fixed m_χ value, an interesting area to focus on is the resonance regime, when $m_{A'} \simeq 2m_\chi$. The decrease of α_D in Fig. 12 could have to do with the fact that the resonance regime can shift due to temperature effects. However, usually the exact dark photon mass that results in a resonance shifts to slightly above twice the DM particle mass, as a result of the relative velocity between the annihilating DM particles, not extended to below that range. Moreover, when looking at the resonance regime the dark photon decay width $\Gamma_{A'}$ is of importance [10]. This decay width is dependent on ε as well as $m_{A'}$ and can be set in the MicrOMEGAs model. Nevertheless, it can not vary while the parameter scans are running, meaning an assumption would have to be made for the value of $m_{A'}$ for the decay width even though the dark photon mass is a variable in the parameter scans. For these dark photon mass ranges, $\Gamma_{A'}$ is of the order of magnitude

of 10^{-3}GeV, meaning if the resonance regime was centered around $2m_\chi$, the whole decrease can not be part of the resonance regime. It could be that near the $2m_\chi$ range another dip in α_D will occur when zooming in on that area. However, because of the relatively small decay width, the results will be very sensitive to changes in $m_{A'}$, making it difficult for the parameter scans to pinpoint the correct $m_{A'}$, α_D pairings signifying this resonance. A search for the resonance regime would fair better if the decay width could vary depending on the dark photon masses from the parameter scans and perhaps by using a parameter scan method that is more efficient in finding the desired parameter combinations as well.

5 Conclusion and Future Research Possibilities

The aim of this research was to see if there are viable DM candidates belonging to the secluded DM model, based off of the current knowledge on the relic abundance of DM in the universe. The results discussed in section 4 show that there are combinations of values for the mass of DM particles and dark photons, as well as the couplings α_D and ε that do result in a relic density close to the value determined by the Planck Collaboration. However, these results are very sensitive to changes in the values chosen for the different parameters.
Moreover, it does appear from these results that a large area of the parameter space can result in the correct relic density, if the correct combinations of values are made. These values then also determine the kinds of interactions that could contribute to the relic density, be it secluded sector annihilations, s-channel annihilations or a combination of the two, as it can be concluded from the results that these are all possibilities.
As there is a vast parameter space that can be covered with the varying parameter combinations, it is more difficult to narrow down possible ranges worth investigating with DM detection searches. However, the values of the variables are so dependant on one and other, influencing the cross section and number density as well, which both play a role in determining the relic abundance. This sensitivity can be advantageous as it provides a clear prediction of where to look when researching a specific parameter space.
This means that there is still plenty of opportunity for further research in the secluded DM model and its interplay with the relic density of DM. For example, an even more detailed look at the relations between the variables of the DM interaction in the secluded DM model can provide further insight in how changes in the values of these parameters will impact the resulting relic density. One proposal would be to perform a scan in all four variable dimensions at once, to pinpoint the exact regions in the parameter space that would provide parameter combinations of secluded DM that result in the correct relic density. By doing this for both annihilation channels, as well as for the region where these channels mix, more knowledge can be gained on in what realistic parameter value region secluded DM could be detected.

6 Acknowledgements

I would like to thank Susanne Westhoff, my supervisor for this research, for introducing me to this subject matter and guiding me through this project. I have learned so much through our many interesting meeting. I would also like to thank Uli Zeitler for being the second reader of this thesis. Lastly, I would also like to thank Jochem Kip for sharing his ABC code with me and helping me with any questions I had regarding programming.

References

[1] N. Aghanim et al. Planck 2018 results. VI. Cosmological parameters. *Astron. Astrophys.*, 641:A6, 2020. [Erratum: Astron.Astrophys. 652, C4 (2021)].

[2] M. Pospelov, A. Ritz, and M.B. Voloshin. Secluded WIMP Dark Matter. *Phys. Lett. B*, 662:53–61, 2008.

[3] G. Bélanger, F. Boudjema, A. Pukhov, and A. Semenov. Doumentation and manual. `https://lapth.cnrs.fr/micromegas/`. Last accessed on 06 July 2023.

[4] What is the universe made of? `https://wmap.gsfc.nasa.gov/universe/uni_matter.html#:~:text=WMAP%20determined%20that%20the%20universe,5.9%20protons%20per%20cubic%20meter.`, Jan 2014. Last accessed 09 July 2023.

[5] A. Riess. Dark matter. `https://www.britannica.com/science/dark-matter`, 2023. Last accessed 04 July 2023.

[6] D. Baumann. *Cosmology*, chapter 3 Thermal History. Institute of Theoretical Physics, University of Amsterdam, (n.d).

[7] P. Gondolo and G. Gelmini. Cosmic abundances of stable particles: Improved analysis. *Nucl. Phys. B*, 360:145–179, 1991.

[8] M. Lisanti. Lectures on Dark Matter Physics. In *Theoretical Advanced Study Institute in Elementary Particle Physics: New Frontiers in Fields and Strings*, pages 399–446, 2017.

[9] Physikalisches Institut Heidelberg. Experimental tests of QED. `https://www.physi.uni-heidelberg.de/~uwer/lectures/StandardModel/Notes/QED-Tests-1.pdf`. Last accessed 15 Juli 2023.

[10] A. Filimonova, S. Junius, L. Lopez Honorez and S. Westhoff. Inelastic dirac dark matter. *Journal of High Energy Physics*, 2022(6), jun 2022.

[11] G. Bélanger, F. Boudjema, A. Pukhov, and A. Semenov. Introduction. `https://lapth.cnrs.fr/micromegas/`. Last accessed on 06 July 2023.

[12] J.P. Lees et al. Search for a dark photon in e^+e^- collisions at babar. *Physical Review Letters*, 113(20), nov 2014.